TIFR/TH/10-11

W^+W^- production in large extra dimension model at next-to-leading order in QCD at the LHC

Neelima Agarwal[a] [1], **V. Ravindran**[b] [2],
Vivek Kumar Tiwari[a] [3], **Anurag Tripathi**[c] [4]

a) Department of Physics, University of Allahabad, Allahabad 211002, India.

b) Regional Centre for Accelerator-based Particle Physics, Harish-Chandra Research Institute, Allahabad 211019, India.

c) Department of Theoretical Physics, Tata Institute of Fundamental Research, Mumbai 400005, India.

Abstract

We present next-to-leading order QCD corrections to production of two W bosons in hadronic collisions in the extra dimension ADD model. Invariant mass and rapidity distributions are obtained to order α_s in QCD by taking into account all the parton level subprocesses. The computation is organized using the monte carlo based method of phase space slicing. We estimate the impact of the QCD corrections on various observables and find that they are significant. We present some results for a 10 TeV LHC but most of the results presented here are for 14 TeV LHC. We also show the reduction in factorization scale uncertainty when $\mathcal{O}(\alpha_s)$ effects are included.

[1] neel1dph@gmail.com
[2] ravindra@hri.res.in
[3] vivekkrt@gmail.com
[4] anurag@theory.tifr.res.in

1 Introduction

The fact that electroweak symmetry breaking scale of the Standard Model (SM) cannot be made stable against the quantum corrections (hierarchy problem) within the SM indicates to the possibility of new physics at TeV scale. The Large Hadron Collider (LHC) which will operate at an enormous center of mass energy ($\sqrt{S} = 14TeV$) offers to shed light on the existence of new physics. The most popular new physics models are based on the ideas of supersymmetry and extra spatial dimensions. Proposals to address the hierarchy problem using extra dimensions were introduced in [1, 2]. In this paper we will consider the model by Arkani-Hamed, Dimopoulos and Dvali (ADD) [1]. In this model all SM fields are confined to a (3+1) dimensional manifold and the extra d spatial dimensions are compactified, with same radius of compactification R, on a d-torii. The effect of extra dimensions appears as Kaluza Klein (KK) gravitons on the 3-brane which couple to SM fields through energy momentum tensor with a strength κ which is related to the volume of the extra dimensions, and the fundamental scale M_s in $4+d$ dimensions by [3]

$$\kappa^2 R^d = 8\pi(4\pi)^{d/2}\Gamma(d/2)M_s^{-(d+2)}. \tag{1}$$

Although the coupling κ is M_{Pl} suppressed, the fact that there are large number of KK modes that couple to the SM fields makes the cumulative effect significant and leads to observable effects. One extra dimension ie. $d = 1$ is ruled out [4] and $d = 2$ is severely constrained so we will consider in this paper $d = 3$ and above. There are two ways to probe such effects at colliders, either through gravitons emission or by virtual graviton exchange. In this paper we will consider only the effects of virtual spin-2 KK states.

The precise measurement of hadronic production of gauge boson pairs is one of the important endeavors at the LHC both in the context of SM and new physics studies. Studies in other channels have been reported in [5] in extra dimension models. In this paper we will consider production of W pair at the LHC. Owing to its importance, its study has attracted a lot of attention in the literature. Many studies have been carried out for its production in the SM; a study in the context of anomalous triple

gauge boson vertices was carried out in [6]. Leading order (LO) studies in the SM can be found in [7]. As is well known the LO results are highly sensitive to the arbitrary renormalization and factorization scales. At this order the factorization scale μ_F enters solely through the parton distribution functions as the parton level cross-section, at this order, does not depend on μ_F. As we include higher order terms of the perturbation series the dependence will reduce and an all order result will be completely independent of these arbitrary scales. In addition the NLO results are usually significantly enhanced as compared to the LO results. It is thus important to carry out NLO calculation to reduce sensitivity to these scales. Because of its importance, W^+W^- production has been studied to next-to-leading-order (NLO) accuracy in the SM [8, 9]. It has also been studied via gluon fusion through a quark box loop or triangle quark loop with γ or Z boson exchange [10] and at one and two loop levels in high energy limit in SM [11]. The significance of NLO computations in the extra dimension models for Drell-Yan [12], diphoton [13], ZZ [14], graviton+photon [15], graviton+jet [16] production has already been demonstrated. These studies show that not only the predictions at NLO are enhanced but are also less sensitive to the factorization scale. With this in mind we carry out a complete NLO calculation of hadronic W^+W^- production in ADD model in this paper. W^+W^- production in Randall Sundrum model is presented in our work [17].

We organize the paper in the following sections as follows. In section 2 we give the details of NLO computation for the W^+W^- production. Here we give the matrix element squares for all the $2 \to 2$ subprocesses both at leading order and at loop level at order a_s $(= g_s^2/16\pi^2)$. All the Feynman diagrams are collected in the appendix. The virtual corrections contain soft and collinear singularities which appear as simple and double poles in ϵ as we use dimensional regularization with $n = 4 + \epsilon$. The $2 \to 3$ real emission matrix elements which were also calculated analytically are not presented here (to save space as the expressions are lengthy) and can be obtained on request. These computations were done using the symbolic manipulation program FORM [18]. We intend to use monte carlo methods for obtaining kinematical distributions. These methods prove

very useful if experimental cuts need to be imposed on the final state particles and they avoid the need for repeating calculations for obtaining different distributions as would be required by completely analytical methods. In this paper we employ the method of two cutoff phase space slicing [19] to carry out our calculation. This method gives numerically stable results as has been demonstrated in [19] and also in our previous works [13, 14]. An alternative to this is dipole subtraction method [20] which is also widely used in higher order QCD calculations. We describe, in brief, phase space slicing method and how the soft and collinear singularities that appear at virtual level and real emission level are treated. In section 3 we present some checks on our code and then present some useful kinematical distributions.

2 Next-to-leading-order Computation

The hadronic production of W bosons at NLO has three pieces of computation. A LO piece which is a $2 \to 2$ parton level process ($q\bar{q} \to W^+W^-$ and $gg \to W^+W^-$); second is the $2 \to 2$ order a_s piece which originates from loop corrections to the LO piece; the third and final part originates from real emission processes where in addition to two W bosons, a parton is also emitted in the final state ($q\bar{q} \to W^+W^-g,\ qg \to W^+W^-q$, and $gg \to W^+W^-g$). Let us take up these three pieces in turn.

2.1 Born Contribution

The charged vector-boson production in the leading partonic scattering processes corresponds to

$$a(p_1) + b(p_2) \to W^+(p_3) + W^-(p_4). \tag{2}$$

where p_1 and p_2 are the momenta of initial state partons while p_3 and p_4 are those of final state vector bosons. The W boson pair can couple to KK gravitons, so it is possible to produce them through virtual graviton exchange at the leading order [21]. In SM this proceeds via t channel (or u channel) quark anti-quark annihilation along with s-channel γ and Z boson exchange shown in Fig. 10. The coupling of fermions to W and Z bosons

are respectively

$$-i\frac{e\mathcal{T}_W}{2}\gamma^\mu\left(1-\gamma^5\right), \qquad -i\frac{e\mathcal{T}_Z}{2}\gamma^\mu\left(C_v-C_a\gamma^5\right). \tag{3}$$

where $\mathcal{T}_\mathcal{W}$ and $\mathcal{T}_\mathcal{Z}$ read

$$\mathcal{T}_W=\frac{1}{\sqrt{2}\sin\theta_W}\,, \qquad \mathcal{T}_Z=\frac{1}{\sin\theta_W\cos\theta_W}. \tag{4}$$

The coefficients C_v and C_a are given by

$$C_v=T_3^f-2\;Q_f\sin^2\theta_W, \qquad C_a=T_3^f, \tag{5}$$

The Q_f and T_3^f denote the electric charge and the third component of the weak isospin of the fermion f respectively, θ_W is the weak mixing angle and m_z is the mass of Z boson. The Z boson propagator is given as

$$\frac{-ig_{\mu\nu}}{s-m_z^2+i\;\Gamma_z m_z}. \tag{6}$$

We have used unitary gauge in the electroweak sector ie. $\xi=\infty$, this simplifies the calculation as both the goldstone boson and ghosts in the electroweak sector disappear.

The γ_5 matrices that appear in the intermediate stages of the computation require special care as they are not defined in arbitrary dimensions. We have used naive anti-commutation relations between γ_5 and other gamma matrices in n dimensions and the resulting traces are then computed in n dimensions as they are free of γ_5. Alternatively, one can use other method namely HVBM-scheme which was proposed in [22] and generalized in [23]. In this approach, Gamma matrices and momenta in the loop and final state phase space integrals are split into a 4 and an $n-4$ dimensional part. The γ_5 anti-commutes in 4 dimensions and commutes in $n-4$ dimensions with rest of the γ matrices.

We give below the matrix element squares summed (averaged) over the final (initial) state spins, colors and polarizations notated by an overline in $n=4+\epsilon$ dimensions . s, t and u are the usual Mandelstam invariants. We will denote by *sm*, *gr* and *int* the

contributions from SM, gravity, and interference of SM with gravity respectively. The SM at LO gives order e^4 contribution to the cross sections:

$$\overline{|M^{(0)}|^2}_{q\overline{q},sm} = \frac{e^4}{N}\left(A_1^q B_1^q + A_2^q B_2^q + A_3^q B_3^q\right) \tag{7}$$

where

$$\begin{aligned}
A_1^u &= \mathcal{T}_W^4 \ , \\
A_2^u &= \frac{e_q^2}{s^2} + e_q\ C_v\ \mathcal{T}_Z\ \cot\theta_W \frac{(s-m_z^2)}{s\left[(s-m_z^2)^2+\Gamma_z^2 m_z^2\right]} \\
&\quad +(C_v^2+C_a^2)\ \mathcal{T}_Z^2\ \cot^2\theta_W \frac{1}{4\left[(s-m_z^2)^2+\Gamma_z^2 m_z^2\right]} \ , \\
A_3^u &= \frac{e_q \mathcal{T}_W^2}{s} + (C_a+C_v)\ \mathcal{T}_W^2\ \mathcal{T}_Z\ \cot\theta_W \frac{(s-m_z^2)}{2\left[(s-m_z^2)^2+\Gamma_z^2 m_z^2\right]} \ .
\end{aligned} \tag{8}$$

A_i^q are in their essence combinations of EW couplings and propagator factors and B_i^q are the functions of the kinematic invariants. N denotes the number of colors. In case of up type quark initiated processes, B_1^u originates from purely t-channel, B_2^u from purely s-channel while B_3^u from the interference of t and s-channel diagrams. These functions are given by

$$\begin{aligned}
B_1^u &= \frac{1}{4m^4t^2}\Big[-\left\{m^8\left(-2+n\right)^2\right\} + t^3u - 2m^2\left(-2+n\right)t^2\left(t+u\right) \\
&\quad +m^4t\left\{\left(-9+4n\right)t+\left(-2+n\right)^2u\right\}\Big] \ ,
\end{aligned} \tag{9}$$

$$\begin{aligned}
B_2^u &= \frac{1}{2m^4}\Big[-20m^8\left(-2+n\right) + 8m^6\left(-2+n\right)\left(t+u\right) + tu\left(t+u\right)^2 \\
&\quad -2m^2\left(-2+n\right)\left(t+u\right)^3 + m^4\Big\{\left(-9+4n\right)t^2 + 2\left(-13+6n\right)tu \\
&\quad +\left(-9+4n\right)u^2\Big\}\Big] \ ,
\end{aligned} \tag{10}$$

$$B_3^u = \frac{1}{2m^4 t}\Bigg[-10m^8\,(-2+n) + 4m^6\,(-2+n)\,(t+u) + t^2 u\,(t+u)$$

$$-2m^2\,(-2+n)\,t\,(t+u)^2 + m^4 t\,\{(-9+4n)\,t + (-13+6n)\,u\}\Bigg] \,. \qquad (11)$$

Here m denotes the mass of final state W bosons. The B_i^q expressions for down type quarks are related to that of up type quarks as follows

$$\begin{aligned} B_1^d\,(t,u,s) &= B_1^u\,(u,t,s)\ , \\ B_2^d\,(t,u,s) &= B_2^u\,(t,u,s)\ , \\ B_3^d\,(t,u,s) &= -B_3^u\,(u,t,s)\ . \end{aligned} \qquad (12)$$

In addition, two more processes are allowed as the KK gravitons can appear at the propagator level, $q\overline{q} \to G^* \to WW$ and $gg \to G^* \to WW$, as shown in Fig. 12. As we use unitary gauge in the electroweak sector the term proportional to $1/\xi$ in the $WW-$graviton vertex [3] drops out. The $q\overline{q}$ and gg initiated contributions which are of order κ^4 are given below.

$$\begin{aligned} \overline{|M^{(0)}|^2}_{q\overline{q},gr} = \frac{1}{64N}|\mathcal{D}_s|^2\kappa^4\Bigg[& n\Big\{8m^8 - 16m^6(t+u) + tu(3t^2+2tu+3u^2) \\ & + m^4(9t^2+30tu+9u^2) - 2m^2(t^3+7t^2u+7tu^2+u^3)\Big\} \\ & - \Big\{8m^8 - 24m^6(t+u) + tu(7t^2+10tu+7u^2) \\ & + m^4(17t^2+62tu+17u^2) - 4m^2(t^3+9t^2u+9tu^2+u^3)\Big\}\Bigg] \,, \end{aligned} \qquad (13)$$

$$\overline{|M^{(0)}|^2}_{gg,gr} = \frac{|\mathcal{D}_s|^2\kappa^4}{(N^2-1)}\frac{1}{128}\times\Bigg[128m^8+9t^4+28t^3u+54t^2u^2+28tu^3+9u^4$$

$$-256m^6(t+u)+192m^4(t+u)^2-64m^2(t+u)^3-\frac{72}{(n-1)^2}s^3(4m^2-s)$$

$$-\frac{3}{n-1}s^2\Big\{188m^4-17t^2-226tu-17u^2+60m^2(t+u)\Big\}$$

$$+\frac{32}{(n-2)^2}\Big\{-44m^8+40m^6(t+u)-40m^2tu(t+u)+9tu(t+u)^2$$

$$+m^4(-9t^2+26tu-9u^2)\Big\}+\frac{4}{n-2}\Big\{692m^8-13t^4-196t^3u-362t^2u^2$$

$$-196tu^3-13u^4-544m^6(t+u)-8m^4(t^2+83tu+u^2)$$

$$+16m^2(5t^3+53t^2u+53tu^2+5u^3)\Big\}\Bigg]\ . \tag{14}$$

We have denoted the sum of spin-2 KK graviton propagators by $\mathcal{D}_s$, then $\mathcal{D}_s$ times square of the coupling can be written as

$$\kappa^2\mathcal{D}_s=\frac{8\pi}{iM_s^4}\left(\frac{\sqrt{s}}{M_s}\right)^{d-2}\left[\pi+2iI(\Lambda/\sqrt{s})\right] \tag{15}$$

The function $I(\Lambda/\sqrt{s})$ depends on the ultraviolet cutoff Λ on the KK modes and its expression can be found in [3]. The default choice for Λ would be the fundamental scale M_s unless mentioned otherwise.

Next we give the interference of SM $q\overline{q}$ process with the gravity mediated $q\overline{q}$ subprocess. For convenience we will denote $M^{(0)}_{q\overline{q},sm}M^{(0)*}_{q\overline{q},gr}+c.\ c.$ by $\overline{|M^{(0)}|^2}_{q\overline{q},int}$.

$$\overline{|M^{(0)}|^2}_{q\overline{q},int} = \frac{e^2\ \kappa^2}{N}\left(C_0^qZ_0^q+C_1^qZ_1^q+C_2^qZ_2^q\right) \tag{16}$$

$$\begin{aligned}
Z_0^u &= \Gamma_z\ m_z\ C_v\ \mathcal{T}_Z\ \cot\theta_W\ \mathcal{I}m\mathcal{D}_s\frac{1}{(s-m_z^2)^2+\Gamma_z^2\ m_z^2}\ ,\\
Z_1^u &= \mathcal{T}_W^2\ \mathcal{R}e\mathcal{D}_s\ , \qquad\qquad (17)\\
Z_2^u &= \mathcal{R}e\mathcal{D}_s\left[C_v\ \mathcal{T}_Z\ \cot\theta_W\frac{(s-m_z^2)}{(s-m_z^2)^2+\Gamma_z^2\ m_z^2}+\frac{2\ Q_u}{s}\right].
\end{aligned}$$

where Z_i^q are in their essence combinations of EW couplings and propagator factors while C_i^q are the functions of kinematic invariants. These C_i^q functions are given below

$$\begin{aligned} C_1^u &= \frac{1}{8m^2t}\Big[4m^8\left(-1+n\right)+t^2\left(t-u\right)u-m^6\left\{\left(-20+11n\right)t+nu\right\}+ \\ &\quad m^4t\left\{\left(-17+8n\right)t+\left(-11+4n\right)u\right\}-m^2t\Big\{2\left(-2+n\right)t^2 \\ &\quad +\left(-4+n\right)tu+\left(-4+n\right)u^2\Big\}\Big]\ , \end{aligned} \tag{18}$$

$$\begin{aligned} C_2^u &= \frac{1}{8m^2}\Big[-10m^6\left(-2+n\right)\left(t-u\right)+m^4\left(-17+8n\right)\left(t^2-u^2\right)+ \\ &\quad tu\left(t^2-u^2\right)-2m^2\left(-2+n\right)\left(t^3-u^3\right)\Big]\ , \end{aligned} \tag{19}$$

$$C_0^u = -C_2^u\ . \tag{20}$$

The C_i^q expressions for down type quarks are related to that of up type quarks as follows.

$$\begin{aligned} C_1^d\left(t,u,s\right) &= C_1^u\left(u,t,s\right)\ , \\ C_2^d\left(t,u,s\right) &= C_2^u\left(t,u,s\right)\ , \\ C_0^d\left(t,u,s\right) &= C_0^u\left(t,u,s\right)\ . \end{aligned} \tag{21}$$

Note that the W boson polarization sum $-g_{\mu\nu}+k_\mu k_\nu/m^2$, which correctly takes into account 3-polarizations of a massive particle, does not give rise to negative powers of m and the $m\to 0$ limit is smooth.

2.2 Radiative Corrections

In Fig. 10, the order a_s loop diagrams that appear in SM and in Fig. 12 the diagrams with a graviton propagator are presented. We will use Feynman gauge $\xi=1$ in the QCD sector and we retain the term proportional to ξ in the gluon-gluon-graviton vertex. However this term does not contribute to the matrix element squares. Here we consider only 5 flavors of quarks and treat them as massless. These diagrams contribute through their interference with the leading order diagrams. In general loop diagrams give ultraviolet divergences

and infrared divergences when the integration over loop momenta is carried out. We use dimensional regularization ($n = 4 + \epsilon$) to regulate these divergences; these divergences then appear as poles in ϵ. Note however that owing to the gauge invariance and the fact that the KK gravitons couple to SM energy momentum tensor, a conserved quantity, this process is UV finite. The external parton leg corrections vanish in dimensional regularization for massless partons. From the loop Feynman diagrams in the appendix we find that all 2-,3-and 4-point loop integrals appear in the calculation. The maximum rank of tensor integrals is 3 and originate from the fermion box. These tensor integrals were reduced to scalar integrals following the procedure of Passarino-Veltman [24]. The 4-point scalar integrals that appear in the gg initiated *box* diagrams were taken from [25]. The one loop matrix elements are recorded below. The finite pieces of matrix element squares denoted by a superscript *fin* are given in the appendix.

The SM contribution is found to be

$$\overline{|M^V|^2}_{q\overline{q},sm} = a_s(\mu_R^2) f(\epsilon, \mu_R^2, s) C_F \left[\Upsilon(\epsilon) \ \overline{|M^{(0)}|^2}_{q\overline{q},sm} + \overline{|M^V|^2}^{fin}_{q\overline{q},sm} \right], \tag{22}$$

the interference of SM with the gravity mediated processes are

$$\overline{|M^V|^2}_{q\overline{q},int} = a_s(\mu_R^2) f(\epsilon, \mu_R^2, s) C_F \left[\Upsilon(\epsilon) \, \overline{|M^{(0)}|^2}_{q\overline{q},int} + \overline{|M^V|^2}^{fin}_{q\overline{q},int} \right] \tag{23}$$

$$\overline{|M^V|^2}_{gg,int} = a_s(\mu_R^2) C_A \left[\overline{|M^V|^2}^{fin}_{gg,int} \right], \tag{24}$$

Note that in the above gg initiated SM diagrams with a quark triangle and γ/Z propagator do not contribute as they vanish in massless limit due to Furry's theorem and weak isospin invariance. Also note that $\overline{|M^V|^2}_{gg,int}$ is completely finite; it does not contain any soft or collinear divergences because in SM the gg contribution begin at the loop level and a lowest order term should be finite.

The pure gravity contributions are

$$\overline{|M^V|^2}_{q\overline{q},gr} = a_s(\mu_R^2) f(\epsilon,\mu_R^2,s) C_F \left[\Upsilon(\epsilon) \overline{|M^{(0)}|^2}_{q\overline{q},gr} + 4(2\zeta(2)-5)\overline{|M^{(0)}|^2}_{q\overline{q},gr} \right] \quad (25)$$

$$\begin{aligned}\overline{|M^V|^2}_{gg,gr} &= a_s(\mu_R^2) f(\epsilon,\mu_R^2,s) C_A \left[\left\{ -\frac{16}{\epsilon^2} + \frac{4}{C_A\epsilon}\left(\frac{11}{3}C_A - \frac{4}{3}n_f T_f\right)\right\} \overline{|M^{(0)}|^2}_{gg,gr} \right. \\ &+ \left. \frac{1}{9}\left(72\zeta(2) + 70\frac{n_f T_f}{C_A} - 203\right)\overline{|M^{(0)}|^2}_{gg,gr} \right] \end{aligned} \quad (26)$$

where

$$\Upsilon(\epsilon) = -\frac{16}{\epsilon^2} + \frac{12}{\epsilon}, \qquad f(\epsilon,\mu_R^2,s) = \frac{\Gamma\left(1+\frac{\epsilon}{2}\right)}{\Gamma(1+\epsilon)}\left(\frac{s}{4\pi\mu_R^2}\right)^{\frac{\epsilon}{2}} \quad (27)$$

The theory is renormalized at scale μ_R. C_F is the Casimir of the fundamental representation while C_A is the Casimir of adjoint representation in the color group.

$$C_F = \frac{N^2-1}{2N}, \qquad C_A = N, \qquad T_f = \frac{1}{2} \quad (28)$$

We can now write the order $a_s(\mu_R^2)$ contributions coming from virtual diagrams as,

$$\begin{aligned} d\sigma^{virt} &= a_s(\mu_R^2) dx_1 dx_2 f(\epsilon,\mu_R^2,s) \\ &\times \left[C_F\left(-\frac{16}{\epsilon^2}+\frac{12}{\epsilon}\right)\sum_i d\sigma^{(0)}_{q_i\overline{q}_i}(x_1,x_2,\epsilon)\left(f_{q_i}(x_1)f_{\overline{q}_i}(x_2) + x_1 \leftrightarrow x_2\right)\right. \\ &+ C_A\left\{-\frac{16}{\epsilon^2}+\frac{4}{C_A\epsilon}\left(\frac{11}{3}C_A - \frac{4}{3}n_f T_F\right)\right\} d\sigma^{(0)}_{gg}(x_1,x_2,\epsilon)\Big(f_g(x_1)f_g(x_2)\Big) \\ &+ C_F\sum_i d\sigma^{V,fin}_{q_i\overline{q}_i}(x_1,x_2,\epsilon)\left(f_{q_i}(x_1)f_{\overline{q}_i}(x_2) + x_1 \leftrightarrow x_2\right) \\ &\left. + C_A\, d\sigma^{V,fin}_{gg}(x_1,x_2,\epsilon)(f_g(x_1)f_g(x_2))\right]. \end{aligned} \quad (29)$$

The poles of order 2 in ϵ in the one loop matrix elements correspond to the configurations which are both soft and collinear simultaneously. These double poles cancel when real emission contributions are included, the remaining simple poles do not cancel completely and are factorized into the bare parton distribution functions at the scale μ_F.

Several checks ensure the correctness of the matrix elements. The W boson polarization sum $-g_{\mu\nu}+k_\mu k_\nu/m^2$, which correctly takes into account 3-polarizations of a massive particle, does not give rise to negative powers of m and the $m \to 0$ limit is smooth. Further, for gluon initiated process the gluon polarization sum is $-g_{\mu\nu} + (k_\mu n_\nu + k_\nu n_\mu)/k.n$ where n is an arbitrary light like vector and the results are independent of the vector n. Furthermore the SM matrix elements are in agreement with the literature [8].

At NLO we also have to include $2 \to 3$ real emission processes. A generic process is of the form

$$a(p_1) + b(p_2) \to W^+(p_3) + W^-(p_4) + c(p_5). \tag{30}$$

In Fig. 11 we show the $q\overline{q}$ and qg initiated real emission Feynman diagrams which appear in SM. In addition, in the ADD model the $2 \to 3$ diagrams with graviton propagator are shown in Fig. 13. Here all the three kinds, $q\overline{q}, qg, gg$ initiated subprocesses occur. The $2 \to 3$ contributions to cross-section reveal the infrared divergences when the integral over the final state particles is carried out. The sum of virtual and real emission cross section is finite after mass factorization is carried out. For details we refer to the review [19].

Although the details of phase space slicing method to deal with soft and collinear singularities in real emission processes were given in our earlier works [13, 14], we shall recapitulate it for completeness. The $2 \to 3$ phase space is divided into soft and collinear regions using two small dimensionless slicing parameters δ_s and δ_c . The soft region is defined as the part of phase space where the final state gluon is soft and has an energy less than $\delta_s\sqrt{s}_{12}/2$ in the center of mass frame of incoming partons. The region complementary to the soft region is hard region and contains collinear singularities. This region is thus further divided into hard collinear region (the region of phase space where the final state parton is collinear to one of the initial state parton) which contains collinear singularities and hard non-collinear region which is free of any singularities. All the order a_s pieces together; the virtual cross-section $d\sigma^{virt}$ the soft piece $d\sigma^{soft}$ and the mass factorized hard collinear contribution $d\sigma^{HC+CT}$ (CT denotes mass factorization

counter term) is referred to as 2-body contribution.

$$d\sigma^{2-body}(\delta_s, \delta_c, \mu_F) = d\sigma^{virt} + d\sigma^{soft}(\delta_s, \delta_c) + d\sigma^{HC+CT}(\delta_s, \delta_c, \mu_F). \quad (31)$$

The only order a_s piece, $d\sigma^{3-body}(\delta_s, \delta_c)$, which remains to be included is hard non collinear and which is finite as the integration over 3-body phase space here does not include soft and collinear regions. The integration over the 3-body phase space is carried out using monte carlo, and it is constrained to avoid collinear and soft regions. The $q\overline{q}$ and gg initiated processes contain both kinds of divergences so the integral is constrained using δ_s and δ_c to avoid these regions. The qg initiated process, however, contain only collinear singularities (as soft fermions do not give singularities) and the 3-body integration is constrained using only δ_c.

The NLO result is sum $d\sigma^{LO} + d\sigma^{2-body}(\delta_s, \delta_c, \mu_F) + d\sigma^{3-body}(\delta_s, \delta_c)$. The sum $d\sigma^{2-body}(\delta_s, \delta_c, \mu_F) + d\sigma^{3-body}(\delta_s, \delta_c)$ constitutes QCD correction, but $d\sigma^{2-body}(\delta_s, \delta_c, \mu_F)$ and $d\sigma^{3-body}(\delta_s, \delta_c)$ independently are not physical quantities as these depend on the (arbitrary) slicing parameters. The sum of these two pieces should be independent of the slicing parameters as these were introduced at the intermediate stages of calculation. We have checked that the sum of 2-body and 3-body contribution is independent of the δ_s and δ_c over a large range of their values.

In the next section we present the results using our monte carlo code which incorporates the above given details. We will present the stability of results against variations of the slicing parameters. This code can easily accommodate any cuts on the final state bosons and can evaluate various kinematical distributions.

3 Kinematical distributions and Results

The LHC with a center of mass energy of 14 TeV will be our default choice. However we will also present some results for a center of mass energy of 10 TeV for the LHC. For numerical evaluation, the following SM parameters [26] are used

$$m_W = 80.398\ GeV, \quad m_Z = 91.1876\ GeV, \quad \Gamma_Z = 2.4952\ GeV, \quad \sin^2\theta_W = 0.231 \quad (32)$$

where θ_W is the weak mixing angle. For the electromagnetic coupling constant α we use $\alpha^{-1} = 128.89$. CTEQ6 [27] density sets are used for parton distribution functions. 2-loop running for the strong coupling constant is used . The number of active massless-quark flavors is taken to be 5 and the value of Λ_{QCD} is chosen as prescribed by the CTEQ6 density sets. At leading order, that is at order α_s^0, we use CTEQ6L1 density set (which uses the LO running a_s) with the corresponding $\Lambda_{QCD} = 165\ MeV$. At NLO we use CTEQ6M density set (which uses 2-loop running a_s) with the $\Lambda_{QCD} = 226\ MeV$; this value of Λ_{QCD} enters into the evaluation of the 2-loop strong coupling. The default choice for the renormalization and factorization scale is the identification to the invariant mass of the W boson pair ie., $\mu_F = \mu_R = Q$. Furthermore the W bosons will be constrained to satisfy $|y_W| < 2.5$, where y_W is the rapidity of a final state W boson .

We will present below the following kinematical distributions:

1. Invariant mass distribution, $d\sigma/dQ$, where Q is the invariant mass of the final state W boson pair,

2. Rapidity distribution $d\sigma/dY$ where $Y = 1/2\ \ln(P_1 \cdot q)/(P_2 \cdot q)$, where P_1 and P_2 are incoming proton momenta and q is the sum of the W boson 4-momenta.

First we demonstrate that the sum of 2-body and 3-body contributions is fairly independent of the slicing parameters. In Fig. 1 (for SM) and Fig. 2 (for signal) we show the variations of these two pieces with the slicing parameters in invariant mass distribution at a value of invariant mass equal to 800 GeV. Here both δ_s and δ_c are varied together with the ratio δ_s/δ_c fixed at a value of 100 [19]. We note that the sum of 2-body and 3-body contributions is fairly stable against variations in these parameters and this gives us confidence in our code. In what follows we will use $\delta_s = 10^{-3}$ and $\delta_c = 10^{-5}$.

In Fig. 3 we have plotted the invariant mass distribution both for the SM and the signal, in the range 300 GeV to 1300 GeV. In this plot we display for three extra dimensions ie., $d = 3$ and for fundamental scale equal to 2 TeV. To highlight the importance of QCD corrections we have also displayed the LO results of SM and the

signal, and we observe that the K factors (defined as $K = d\sigma^{NLO}/d\sigma^{LO}$) are significantly large. We note that for the signal $(sm + gr + int)$ K factor varies between 1.55 to 1.98 in the invariant mass range of 300 to 1300 GeV. This also shows that the LO results can be only treated as first approximations and to have more precise estimates we should go beyond the leading order. We note here that present computation does not take into account decay of W bosons to leptons which is observed experimentally, but as QCD corrections are independent of these decays, the K factors obtained here would not change when decays are taken into account.

To estimate the effect of the number of extra dimension on the invariant mass distribution, we plot in Fig. 4 the signal for three different values of d (3,4,5) with M_s fixed at 2 TeV. We note that the lower the value of d, more is the strength of the signal. Next in Fig. 5 we have plotted $d\sigma/dQ$ for three different values of M_s (2.0, 2.5, 3.0) at a fixed value 3 for the number of extra dimensions. As expected, with increase in the fundamental scale the deviations from SM predictions become less, and significant deviations from SM are observed at higher energies still. Next, in Fig. 6 we present the effect of variation of the UV cutoff Λ that appears in the expression of graviton propagator (see eq. 15) for $M_s = 3TeV$ and $d = 3$. We observe that lowering the cutoff from M_s by 25% lowers the predictions by 14%.

In Fig. 7 we have plotted the rapidity distribution $d\sigma/dY$ at LO and NLO both for SM and the signal for $d = 3$ and M_s fixed at 2 TeV. We have plotted this distribution in the interval $-2.0 < Y < 2.0$ and have carried out an integration over the invariant mass interval $900 < Q < 1100$ to increase the signal over the SM background. As expected the distribution is symmetric about $Y = 0$.

As was noted before the NLO QCD corrections reduce the sensitivity of the cross sections to the factorization scale μ_F; this we now show in the Fig. 8. We have plotted SM and the signal both at LO and NLO, and have varied the factorization scale μ_F in the range $Q/2 < \mu_F < 2Q$. The central curve in a given band (shown by the dotted curves) correspond to $\mu_F = Q$. In all these the renormalization scale is fixed at $\mu_R = Q$. We

notice that the factorization scale uncertainties in SM are less compared to the signal. This is because of the dominant role of the gluon gluon initiated process in the signal. We see in this figure that a significant reduction in theoretical uncertainty, arising from the factorization scale, is achieved by our NLO computation. At $Q = 1300\ GeV$ the $d\sigma/dQ$ for the signal varies by 18.8 % at LO as μ_F is varied between $Q/2$ to $2Q$ and it varies by 7.6 % at NLO. At the end we present in Fig. 9, $d\sigma/dQ$ for LHC with a centre of mass energy of 10 TeV at NLO both for SM and signal. For comparison we have also plotted the 14 TeV results in the same figure.

4 Conclusions

In this paper we undertook computation of W boson pair production at the LHC at next-to-leading order in QCD in the extra dimension model of ADD. Here only spin-2 KK gravitons appearing at the propagator level were considered. W boson production is one of the important channels at the LHC to probe both the standard model and new physics. As the leading order results serve only as first approximations we need to go beyond it to NLO to have more precise estimates. The NLO results are generally not only significantly larger as compared to the LO results but they are also much less sensitive to the arbitrary factorization scale and renormalization scale (if the LO already starts at order a_s).

Here we carried out a full NLO computation and presented analytical expressions of matrix element squares for all the SM, gravity mediated and the interference of SM and gravity mediated processes both at the LO and virtual level. We used dimensional regularization to regulate soft and collinear divergences and the singularity structure in the loop level matrix elements is shown and it is observed that the singular pieces are proportional to the born contributions. As different kinematical distributions such as invariant mass distribution and rapidity distribution are evaluated with cuts on the final state W bosons it is useful to use monte carlo based semi analytical methods which allow to tailor code easily to these requirements. For this we used the two cutoff phase

space slicing method to divide phase space in soft and collinear regions and filter out the singularities in the real emission contributions which appear on phase space integrations. A brief discussion on this method was presented. To save space we omitted the real emission matrix elements as the expressions are voluminous and can be obtained on request. We have used $\overline{M}S$ scheme throughout this paper.

We have presented distributions for the LHC at $14TeV$ and $10TeV$. We first offered some checks on our monte carlo code such as stability of sum of $2-body$ and $3-body$ contributions against variation of the slicing parameters δ_s and δ_c and then presented invariant mass and rapidity distributions both at LO and NLO. We use CTEQ 6L1 and CTEQ 6M parton density sets for LO and NLO observables, respectively. Significant enhancements over the LO predictions are observed. The K factors are found to be large in the invariant mass distribution. For LHC at $14TeV$ we find that K factor in the invariant mass distribution for the signal $(sm + gr + int)$ varies between 1.55 and 1.98 as Q varies between 300 to 1300 GeV. We have shown that a significant reduction in theoretical uncertainty, arising from the factorization scale, is achieved by our NLO computation. At $Q = 1300\ GeV$ the $d\sigma/dQ$ varies by 18.8 % at LO as μ_F is varied between $Q/2$ to $2Q$ and it varies by 7.6 % at NLO. These observations justify the entire exercise and give results that are precise and suitable for further studies for constraining the parameters of the ADD model. Invariant mass distribution is also presented for LHC at a center of mass energy of $10TeV$ at the NLO level.

Acknowledgments: The work of NA is supported by CSIR Senior Research Fellowship, New Delhi. NA, AT and VR would also like to thank the cluster computing facility at Harish-Chandra Research Institute. NA and VKT acknowledge the computational support of the computing facility which has been developed by the Nuclear Particle Physics Group of the Physics Department, Allahabad University under the Center of Advanced Study (CAS) funding of U.G.C. India. The authors would like to thank Prakash Mathews and M.C. Kumar for useful discussions.

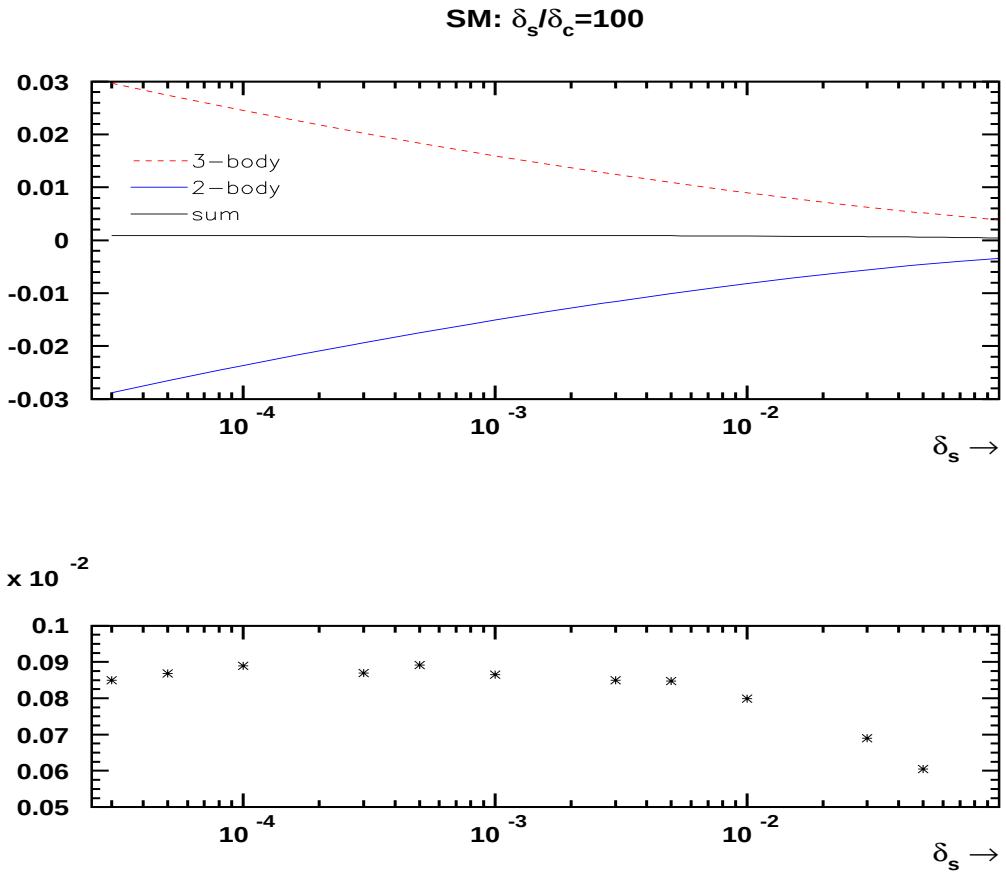

Figure 1: Variation of 2-body and 3-body contributions (of $d\sigma/dQ$ at $Q = 800\ GeV$ in SM) and their sum with δ_s. Here $\delta_s/\delta_c = 100$ has been used.

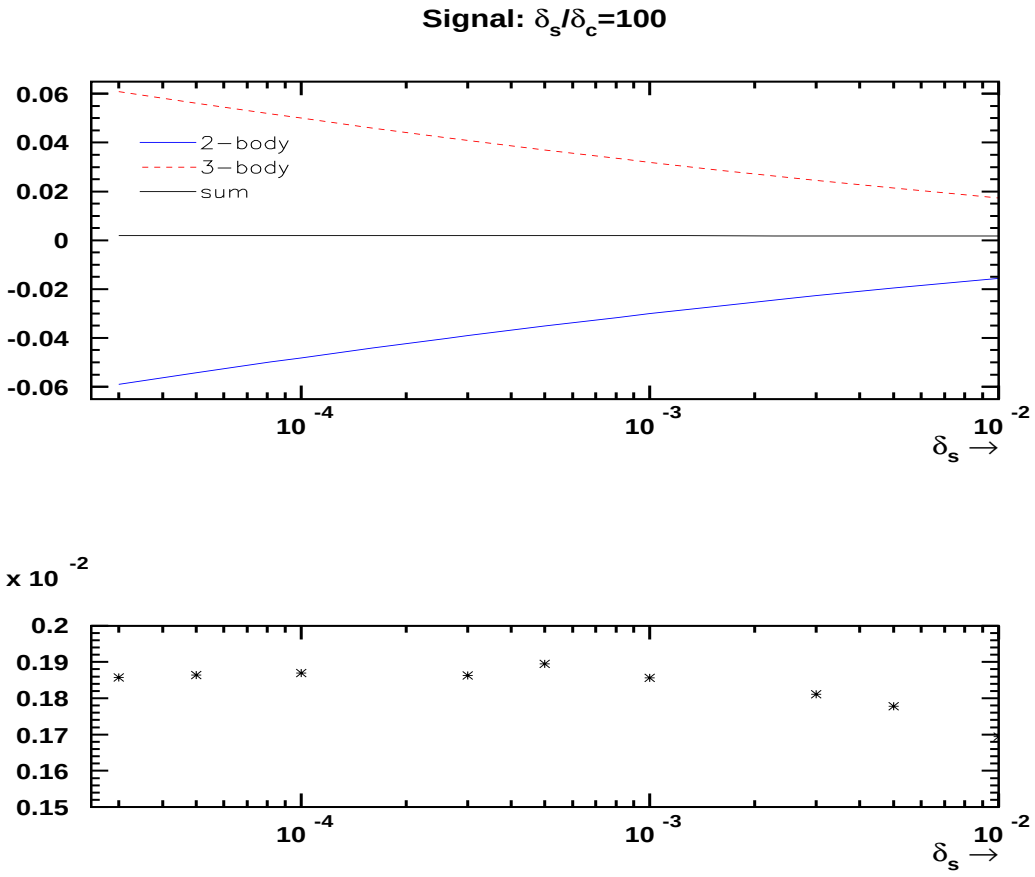

Figure 2: Variation of 2-body and 3-body contributions (of $d\sigma/dQ$ at $Q = 800GeV$ in signal) and their sum with δ_s. Here $\delta_s/\delta_c = 100$ has been used.

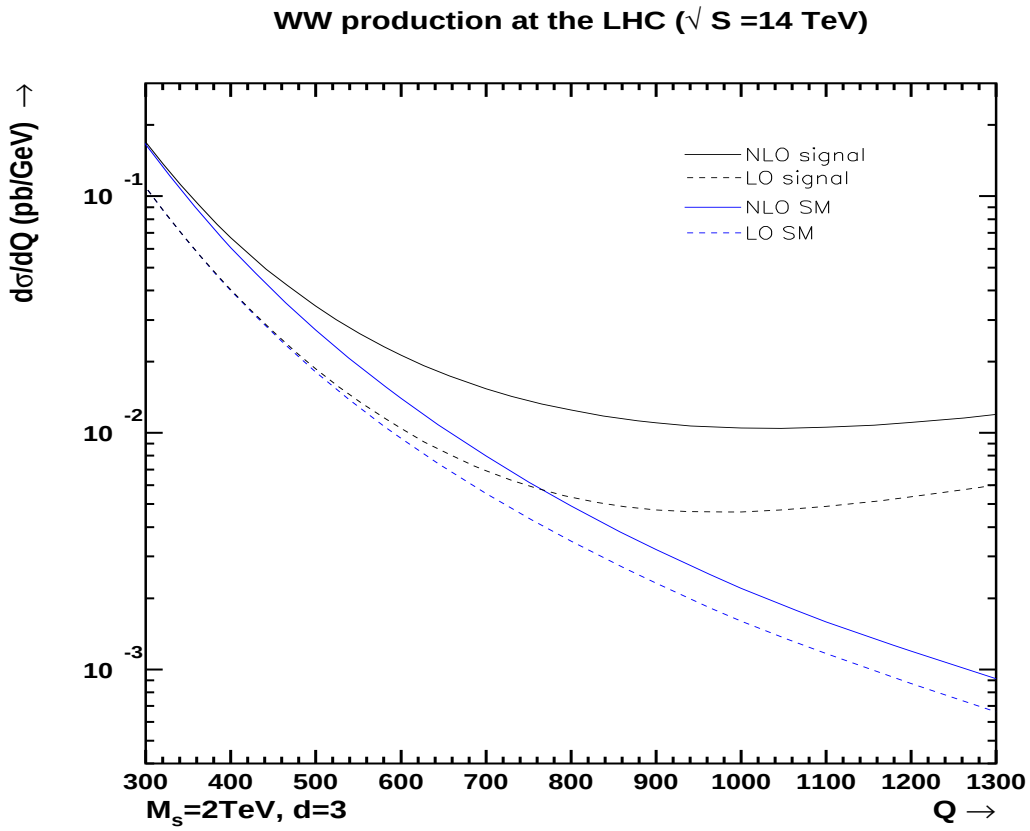

Figure 3: Invariant mass distribution at LO and NLO in SM and for the signal at $M_s = 2TeV$ and 3 extra dimensions.

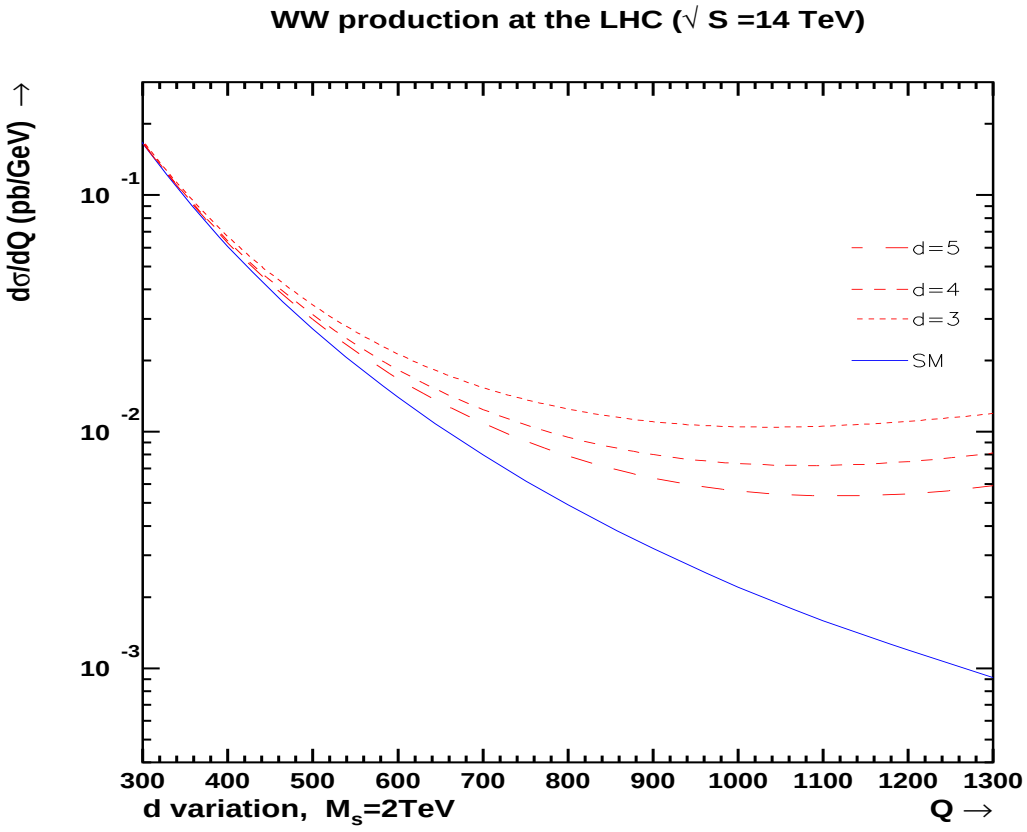

Figure 4: Effect of variation of number of extra dimensions in invariant mass distribution. The fundamental scale M_s has been fixed at 2 TeV. The curves correspond to NLO results.

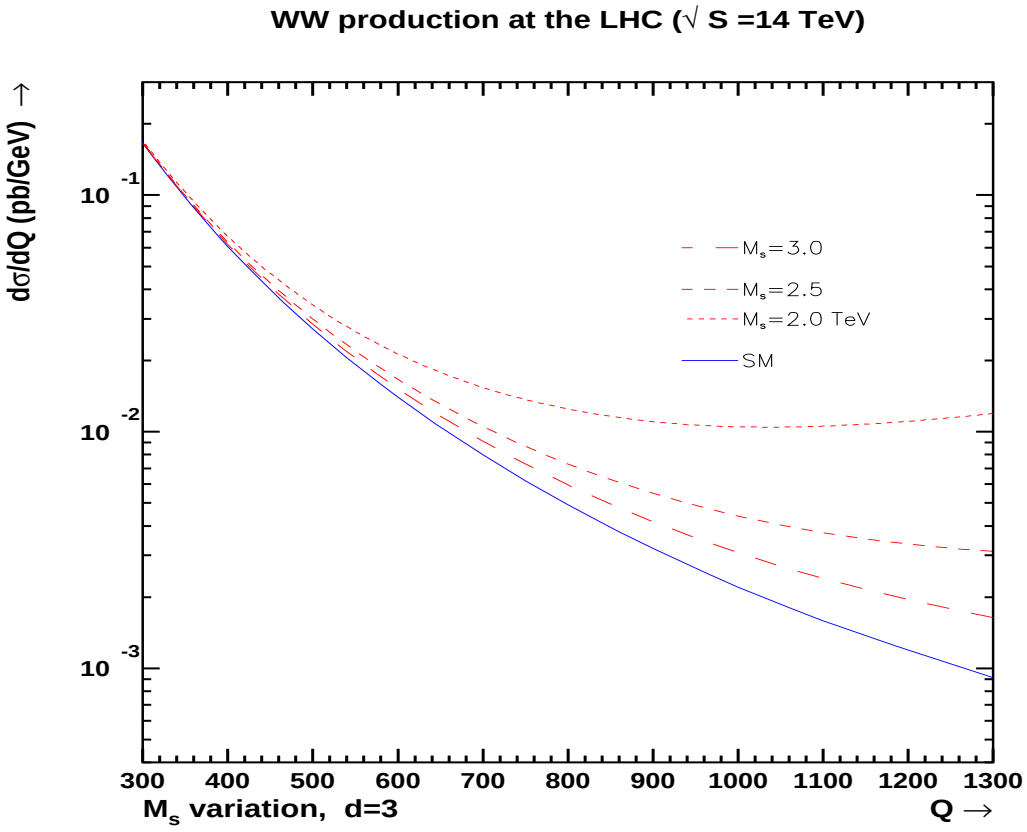

Figure 5: Effect of variation of the fundamental scale M_s in the invariant mass distribution. The number of extra dimensions has been fixed at 3. The curves correspond to NLO results.

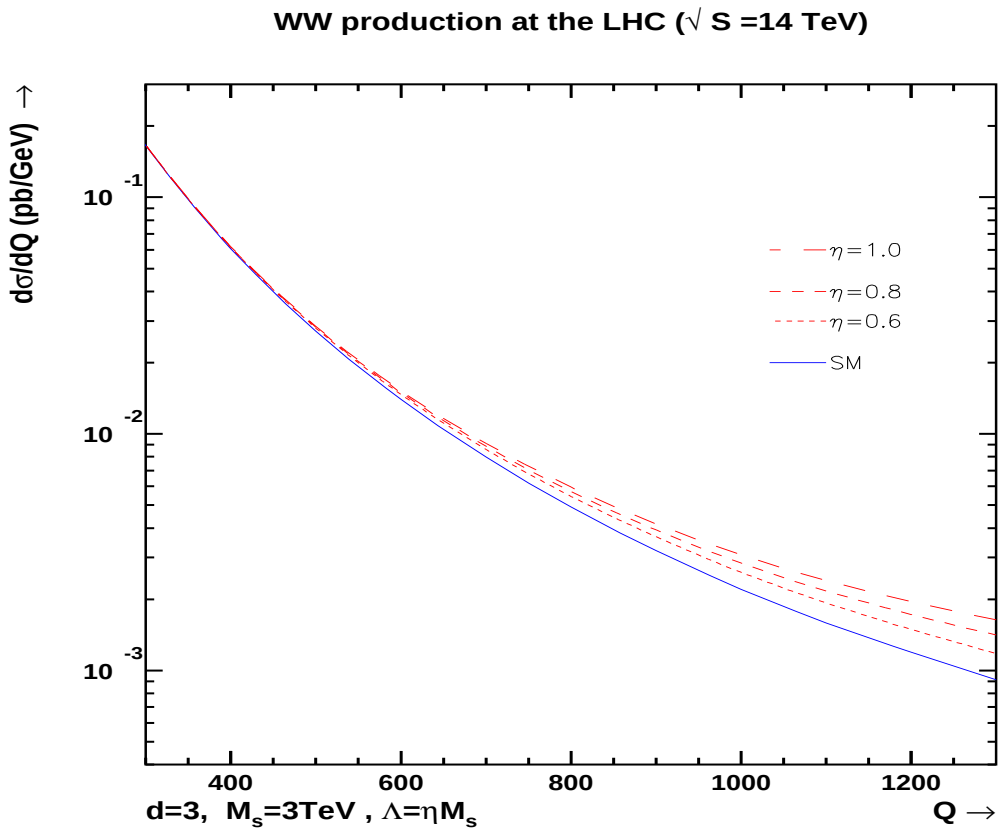

Figure 6: Effect of variation of the UV cutoff scale Λ in the invariant mass distribution for $d = 3$ and $M_s = 3TeV$. The curves correspond to NLO results.

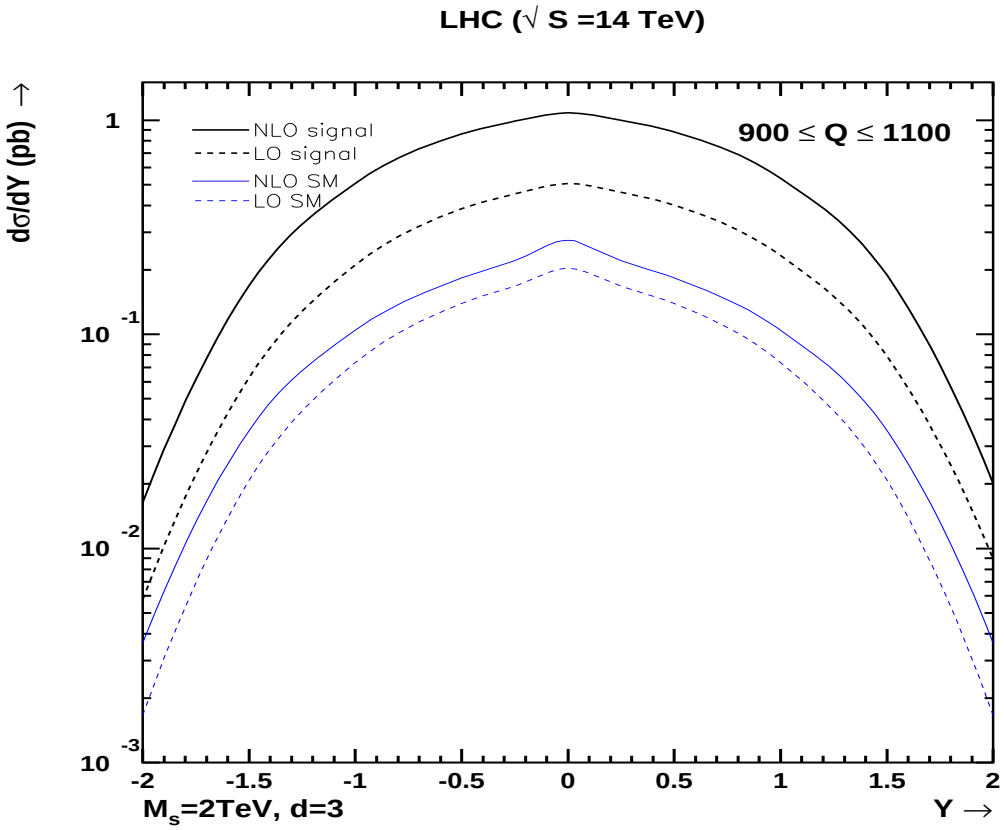

Figure 7: Rapidity distribution for $M_s = 2TeV$ for SM and signal for $d = 3$. We have integrated over the invariant mass range $900 < Q < 1100$ to enhance the signal.

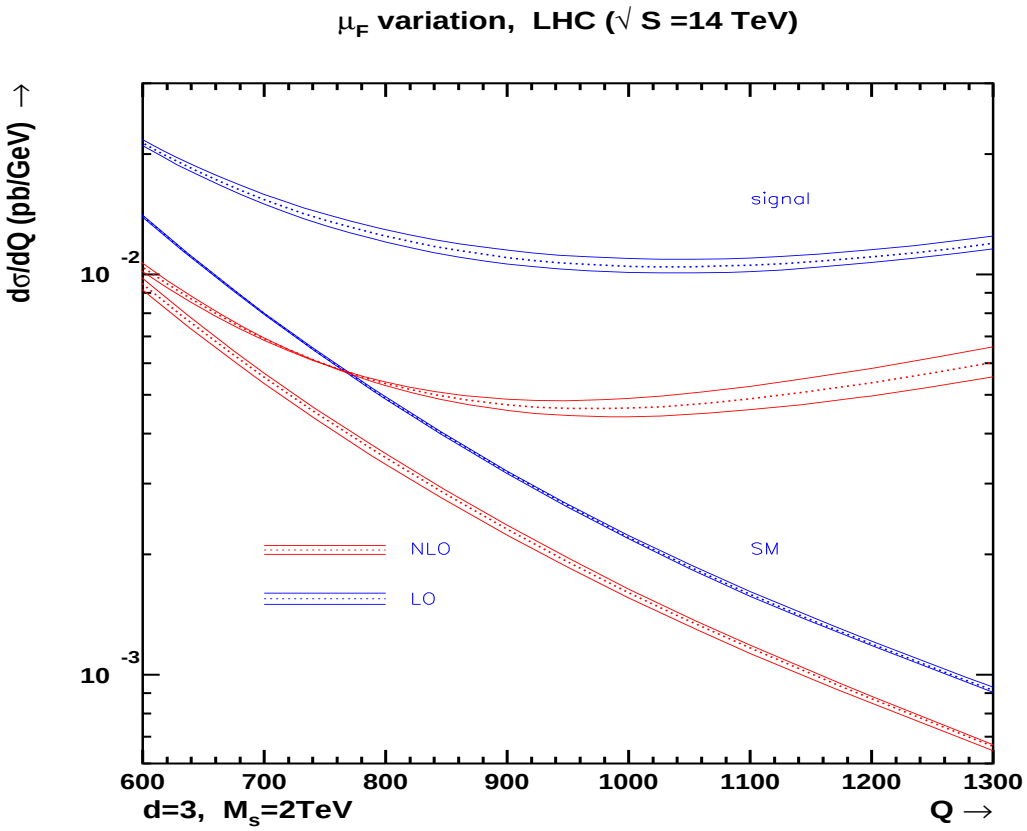

Figure 8: Factorization scale variation in the invariant mass distribution. The number of extra dimensions $d = 3$ and the fundamental scale $M_s = 2TeV$ have been chosen.

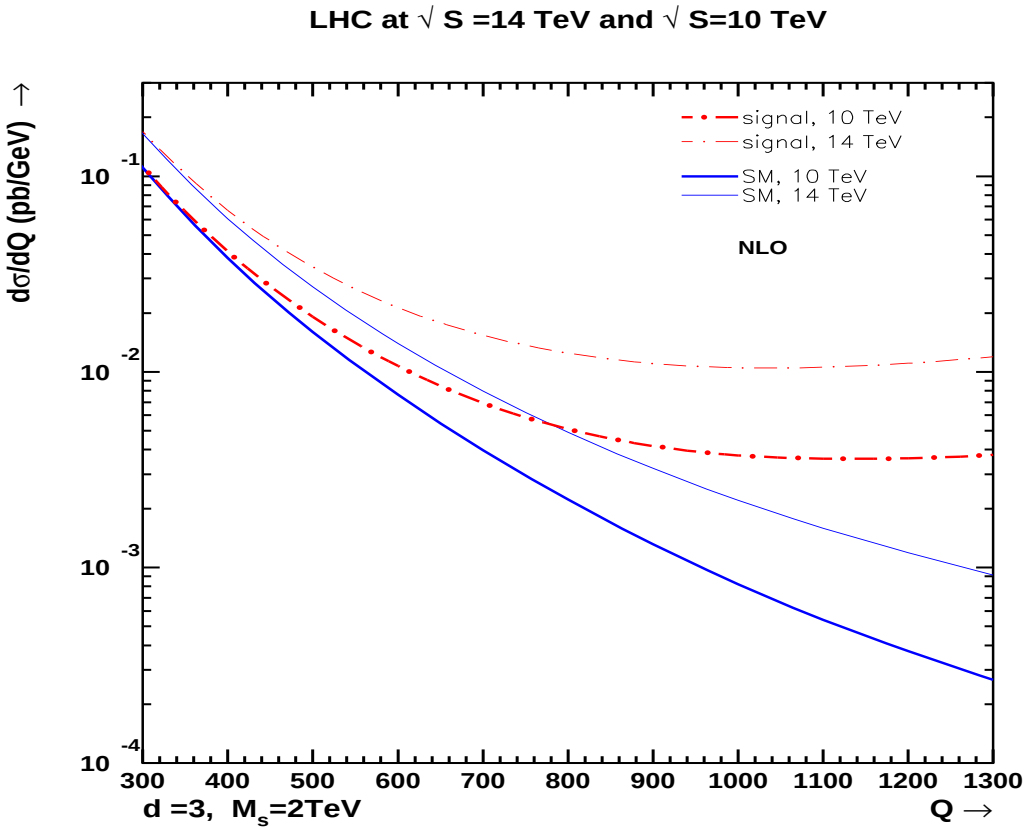

Figure 9: Invariant mass distribution at NLO for SM and the signal. Here the thicker curves correspond to $\sqrt{S} = 10TeV$ and lighter curves to $\sqrt{S} = 14TeV$ at the LHC.

References

[1] I. Antoniadis, N. Arkani-Hamed, S. Dimopoulos and G. R. Dvali, Phys. Lett. B **436**, 257 (1998) [arXiv:hep-ph/9804398]; N. Arkani-Hamed, S. Dimopoulos and G. R. Dvali, Phys. Lett. B **429**, 263 (1998) [arXiv:hep-ph/9803315].

[2] L. Randall and R. Sundrum, Phys. Rev. Lett. **83**, 3370 (1999) [arXiv:hep-ph/9905221]; L. Randall and R. Sundrum, Phys. Rev. Lett. **83**, 4690 (1999) [arXiv:hep-th/9906064].

[3] T. Han, J. D. Lykken and R. J. Zhang, Phys. Rev. D **59** (1999) 105006 [arXiv:hep-ph/9811350]. G. F. Giudice, R. Rattazzi and J. D. Wells, Nucl. Phys. B **544** (1999) 3 [arXiv:hep-ph/9811291].

[4] D. J. Kapner, T. S. Cook, E. G. Adelberger, J. H. Gundlach, B. R. Heckel, C. D. Hoyle and H. E. Swanson, Phys. Rev. Lett. **98**, 021101 (2007) [arXiv:hep-ph/0611184].

[5] P. Mathews, S. Raychaudhuri and K. Sridhar, JHEP **0007**, 008 (2000) [arXiv:hep-ph/9904232]; K. Hagiwara, P. Konar, Q. Li, K. Mawatari and D. Zeppenfeld, JHEP **0804**, 019 (2008) [arXiv:0801.1794 [hep-ph]]; S. Lola, P. Mathews, S. Raychaudhuri and K. Sridhar, arXiv:hep-ph/0010010; M. Kober, B. Koch and M. Bleicher, Phys. Rev. D **76**, 125001 (2007) [arXiv:0708.2368 [hep-ph]]; J. Gao, C. S. Li, X. Gao and J. J. Zhang, Phys. Rev. D **80**, 016008 (2009) [arXiv:0903.2551 [hep-ph]].

[6] K. Hagiwara, R. D. Peccei, D. Zeppenfeld and K. Hikasa, Nucl. Phys. B **282** (1987) 253. U. Baur, T. Han and J. Ohnemus, Phys. Rev. D **53**, 1098 (1996) [arXiv:hep-ph/9507336].

[7] R. W. Brown and K. O. Mikaelian, Phys. Rev. D **19** (1979) 922.

[8] J. Ohnemus, Phys. Rev. D **44**, 1403 (1991); S. Frixione, Nucl. Phys. B **410**, 280 (1993).

[9] J. Ohnemus, Phys. Rev. D **50**, 1931 (1994) [arXiv:hep-ph/9403331]; L. J. Dixon, Z. Kunszt and A. Signer, Nucl. Phys. B **531**, 3 (1998) [arXiv:hep-ph/9803250]; L. J. Dixon, Z. Kunszt and A. Signer, Phys. Rev. D **60**, 114037 (1999) [arXiv:hep-ph/9907305]; J. M. Campbell and R. K. Ellis, Phys. Rev. D **60**, 113006 (1999) [arXiv:hep-ph/9905386].

[10] C. Kao and D. A. Dicus, Phys. Rev. D **43**, 1555 (1991); G. Davatz, G. Dissertori, M. Dittmar, M. Grazzini and F. Pauss, JHEP **0405**, 009 (2004) [arXiv:hep-ph/0402218]; M. Duhrssen, K. Jakobs, J. J. van der Bij and P. Marquard, JHEP **0505**, 064 (2005) [arXiv:hep-ph/0504006]; T. Binoth, M. Ciccolini, N. Kauer and M. Kramer, JHEP **0612**, 046 (2006) [arXiv:hep-ph/0611170]; E. Accomando, Phys. Lett. B **661**, 129 (2008) [arXiv:0709.1364 [hep-ph]].

[11] G. Chachamis, M. Czakon and D. Eiras, arXiv:0806.3043 [hep-ph]; G. Chachamis, M. Czakon and D. Eiras, JHEP **0812**, 003 (2008) [arXiv:0802.4028 [hep-ph]].

[12] P. Mathews, V. Ravindran, K. Sridhar and W. L. van Neerven, Nucl. Phys. B **713**, 333 (2005) [arXiv:hep-ph/0411018]; P. Mathews, V. Ravindran and K. Sridhar, JHEP **0510**, 031 (2005) [arXiv:hep-ph/0506158]; P. Mathews and V. Ravindran, Nucl. Phys. B **753**, 1 (2006) [arXiv:hep-ph/0507250]; M. C. Kumar, P. Mathews and V. Ravindran, Eur. Phys. J. C **49**, 599 (2007) [arXiv:hep-ph/0604135].

[13] M. C. Kumar, P. Mathews, V. Ravindran and A. Tripathi, Phys. Lett. B **672**, 45 (2009) [arXiv:0811.1670 [hep-ph]]; M. C. Kumar, P. Mathews, V. Ravindran and A. Tripathi, Nucl. Phys. B **818**, 28 (2009) [arXiv:0902.4894 [hep-ph]].

[14] N. Agarwal, V. Ravindran, V. K. Tiwari and A. Tripathi, arXiv:0909.2651 [hep-ph]; N. Agarwal, V. Ravindran, V. K. Tiwari and A. Tripathi, arXiv:0910.1551 [hep-ph].

[15] X. Gao, C. S. Li, J. Gao, R. J. Oakes and J. Wang, arXiv:0912.0199 [hep-ph].

[16] S. Karg, M. Kramer, Q. Li and D. Zeppenfeld, arXiv:0911.5095 [hep-ph].

[17] N. Agarwal, V. Ravindran, V. K. Tiwari and A. Tripathi, arXiv:1003.5445 [hep-ph].

[18] J. A. M. Vermaseren, arXiv:math-ph/0010025.

[19] B. W. Harris and J. F. Owens, Phys. Rev. D **65**, 094032 (2002) [arXiv:hep-ph/0102128].

[20] S. Catani and M.H. Seymour, Phys. Lett. B **378**, 287 (1996) [arXiv:hep-ph/9602277]; Nucl. Phys. B **485**, 291 (1997) [Erratum-ibid. B **510**, 503 (1997)] [arXiv:hep-ph/9605323].

[21] K. Agashe, H. Davoudiasl, G. Perez and A. Soni, Phys. Rev. D **76**, 036006 (2007) [arXiv:hep-ph/0701186]. K. Agashe, S. Gopalakrishna, T. Han, G. Y. Huang and A. Soni, Phys. Rev. D **80**, 075007 (2009) [arXiv:0810.1497 [hep-ph]]. O. Antipin, D. Atwood and A. Soni, Phys. Lett. B **666**, 155 (2008) [arXiv:0711.3175 [hep-ph]].

[22] G. 't Hooft and M. J. G. Veltman, Nucl. Phys. B **44** (1972) 189;

[23] P.Breitenlohner, B. Maison, Commun.Math.53 (1977) 11, P.Breitenlohner, B. Maison, Commun.Math.53 (1977) 39, P.Breitenlohner, B. Maison, Commun.Math.53 (1977) 55.

[24] G. Passarino and M. J. G. Veltman, Nucl. Phys. B **160**, 151 (1979).

[25] G. Duplancic and B. Nizic, Eur. Phys. J. C **20**, 357 (2001) [arXiv:hep-ph/0006249]; Z. Bern, L. J. Dixon and D. A. Kosower, Nucl. Phys. B **412**, 751 (1994) [arXiv:hep-ph/9306240].

[26] C. Amsler *et al.* [Particle Data Group], Phys. Lett. B **667**, 1 (2008).

[27] J. Pumplin, D. R. Stump, J. Huston, H. L. Lai, P. M. Nadolsky and W. K. Tung, JHEP **0207** (2002) 012 [arXiv:hep-ph/0201195]; D. Stump, J. Huston, J. Pumplin, W. K. Tung, H. L. Lai, S. Kuhlmann and J. F. Owens, JHEP **0310** (2003) 046 [arXiv:hep-ph/0303013].

5 Appendix

Below we give the finite pieces of the matrix element squares that appear in Eq. 22 through Eq. 24 in section 2.

$$\overline{|M^V|^2}^{fin}_{q\bar{q},sm} = \frac{e^4}{N}\left[A_0^q B_0^q + A_1^q B_{11}^q + A_2^q B_{22}^q + A_3^q B_{33}^q\right] \tag{33}$$

where A_i^q contain the coupling and propagator factors , B_i^q are the functions of the kinematic invariants.

$$A_0^u = \frac{1}{2\pi}\frac{(C_a + C_v)\ \Gamma_z\ m_z\ \mathcal{T}_W^2\ \mathcal{T}_Z\ \cot\theta_W}{(s-m_z^2)^2 + \Gamma_z^2 m_z^2} \tag{34}$$

and the rest A_i^q are given in eqn. (8). The B_i^q functions are as follows.

$$\begin{aligned} B_0^u &= \frac{12}{t}\Big[2G_1\left(10m^4 - 4m^2(2t+u) + t(2t+u)\right) \\ &\quad -\frac{1}{(m^2-t)^2}\Big\{\zeta(2)\Big(15m^8 - 6m^6(2t+u) - t^2u(t+2u) - 3m^4t(t+3u) \\ &\quad +2m^2t(t^2+6tu+2u^2)\Big)\Big\}\Big]\ , \end{aligned} \tag{35}$$

$$\begin{aligned} B_{11}^u &= \frac{2G_2}{t^2}\left(-2m^4+tu\right) + 2\zeta(2)\left\{7 - \frac{8m^4}{t^2} + \frac{6u}{t} + \frac{tu}{m^4} - \frac{4(t+u)}{m^2}\right\} \\ &\quad +\frac{G_3}{(m^2-t)t^2}\Big\{6m^6 + 6m^4t - 2t^2u - 2m^2t(2t+3u)\Big\} \\ &\quad +\frac{2(2m^2+t+u)}{m^4(-4m^2+s)^2t^2}\Big\{18m^{10} - 2t^3u(t+u) + m^8(11t+9u) - 2m^6t(14t+9u) \\ &\quad +m^4t(2t^2-9tu-9u^2) + 4m^2t^2(2t^2+3tu+2u^2)\Big\} + \frac{G_4}{(-4m^2+s)^2t^2} \\ &\quad \Big\{24m^8 + 8m^6(t+3u) + 2t(t-u)(t+u)(2t+3u) + 4m^2t(t^2-6tu-3u^2) \\ &\quad +m^4(-22t^2-8tu+6u^2)\Big\} + \frac{2G_5}{s(-4m^2+s)^2t}\Big\{-12m^8 + 4m^6(s+2t) \\ &\quad +su(t+u)^2 + 2m^2su(3t+u) + 2m^4(2t^2+s(t+u))\Big\}\ , \end{aligned} \tag{36}$$

$$B^u_{22} = \frac{1}{m^4}\Big[-4(-2+\zeta(2))\Big\{40m^8 - 16m^6(t+u) - tu(t+u)^2 + 4m^2(t+u)^3$$
$$-m^4(7t^2+22tu+7u^2)\Big\}\Big] \ , \tag{37}$$

$$B^u_{33} = 2\Big[-\frac{G_2}{t}\Big\{10m^4 - 4m^2(2t+u) + t(2t+u)\Big\} + \frac{2\zeta(2)}{m^4 t}\Big\{ -30m^8$$
$$+t^2u(t+u) - 4m^2t(t+u)^2 + 5m^4t(t+2u) + 4m^6(4t+3u)\Big\}$$
$$+\frac{G_3}{t(m^2-t)^2}\Big\{15m^8 - 6m^6(2t+u) - t^2u(t+2u) - 3m^4t(t+3u)$$
$$+2m^2t(t^2+6tu+2u^2)\Big\} + \frac{G_5}{s(-4m^2+s)^2}\Big\{ -32m^8 + 4m^6(11s+8t)$$
$$-s(t+u)^2(2t+u) + 2m^4s(5t+17u) + 2m^2s(-2t^2+tu+3u^2)\Big\}$$
$$+\frac{G_4(2m^2+t+u)}{t(-4m^2+s)^2}\Big\{30m^6 + m^4(-13t+3u) + t(t+u)(2t+3u)$$
$$-2m^2(t^2+11tu+3u^2)\Big\} + \frac{(2m^2+t+u)^2}{m^4(-4m^2+s)^2(m^2-t)t}\Big\{85m^{10}$$
$$+m^6t(4t-17u) + 4t^3u(t+u) - 4m^2t^2(t+u)(4t+5u)$$
$$-m^8(115t+34u) + m^4t(44t^2+79tu+18u^2)\Big\}\Big] \ . \tag{38}$$

$$\overline{|M^V|^2}^{fin}_{q\bar{q},int} \;\; = \;\; = \frac{e^2\kappa^2}{N}\left[C^q_{00}Z^q_0 + C^q_{11}Z^q_1 + C^q_{22}Z^q_2 + C^q_{33}Z^q_3\right] \tag{39}$$

where Z^q_i contain the coupling and propagator factors while C^q_i are the functions of kinematic invariants.

$$Z^u_3 = \mathcal{T}^2_W \; \pi \; \mathcal{I}m\mathcal{D}_s \tag{40}$$

and rest Z^q_i are given in eqn. (17). The C^q_i functions are as follows.

$$\begin{aligned}
C^u_{11} \;\; = \;\; & \frac{1}{4}\Big[\frac{2G_3}{t(m^2-t)}\Big\{-9m^8-4m^4t^2+3m^6(5t+u)-m^2tu(9t+u)+t^2u(2t+3u)\Big\} \\
& +4G_8\Big\{\frac{-3m^6}{t}+t^2+m^2\left(-5t-\frac{7u}{2}\right)+tu+\frac{u^2}{2}+m^4\left(8+\frac{u}{t}\right)\Big\} \\
& -\frac{4G_6}{t}\Big\{-6m^6+2m^4(8t+u)-m^2t(10t+7u)+t(2t^2+2tu+u^2)\Big\} \\
& +\frac{4\zeta(2)}{m^2t}\Big\{18m^8+t^2(t-u)u-2m^6(20t+3u)+m^4t(25t+12u) \\
& -m^2t(6t^2+2tu+u^2)\Big\}-\frac{2G_5}{s(-4m^2+s)^2}\Big\{-32m^{10}+16m^8(3s+4t) \\
& +m^6(-42st-32t^2+34su)-4m^4s(4t^2+10tu-u^2)+s(t+u)^2(2t^2+2tu+u^2) \\
& +m^2s(2t^3-3t^2u-6tu^2-u^3)\Big\}+\frac{2G_4}{(-4m^2+s)^2t}\Big\{-36m^{10}+4m^8(13t-6u) \\
& +m^2t(2t-9u)(t+u)^2+tu(t+u)^2(2t+3u)+m^6(-5t^2+66tu+3u^2) \\
& +m^4(-4t^3-49t^2u+2tu^2+3u^3)\Big\}+\frac{1}{(-4m^3+ms)^2t}\Big\{-456m^{12} \\
& +8m^{10}(55t-38u)-9t^2(t-u)u(t+u)^2+m^8(226t^2+648tu+38u^2) \\
& +m^4t(9t^3-217t^2u-201tu^2-47u^3)-2m^6(90t^3+129t^2u-64tu^2-19u^3) \\
& +2m^2t(18t^4+18t^3u+17t^2u^2+16tu^3-u^4)\Big\}\Big] \;, \qquad (41)
\end{aligned}$$

$$
\begin{aligned}
C_{22}^u &= \frac{(4\zeta(2)-9)(t-u)}{4m^2}\Big[-20m^6+15m^4(t+u)+tu(t+u) \\
&\quad -4m^2(t^2+tu+u^2)\Big] \,, \qquad (42)
\end{aligned}
$$

$$
\begin{aligned}
C_{33}^u &= \frac{2}{4t}\Big[\frac{1}{m^2-t}\Big\{-9m^8-4m^4t^2+3m^6(5t+u) \\
&\quad -m^2tu(9t+u)+t^2u(2t+3u)\Big\} \\
&\quad -2(G_7-G_3)\Big\{-6m^6+2m^4(8t+u)-m^2t(10t+7u) \\
&\quad +t(2t^2+2tu+u^2)\Big\}\Big] \,, \qquad (43)
\end{aligned}
$$

$$
C_{00}^u = -C_{22}^u \,. \qquad (44)
$$

where

$$
\begin{aligned}
G_1 &= \zeta(2)\ln\left(\frac{(t-m^2)^2}{m^2s}\right)-\ln\left(-\frac{t}{m^2}\right) \,, \\
G_2 &= 2\ln\left(-\frac{t}{m^2}\right)\ln\left(\frac{(t-m^2)^2}{m^2s}\right)+4Li_2\left(\frac{t}{m^2}\right)-\ln^2\left(\frac{-t}{m^2}\right) \,, \\
G_3 &= \ln\left(-\frac{t}{m^2}\right) \,, \qquad G_4=\ln\left(\frac{s}{m^2}\right) \,, \\
G_5 &= \frac{1}{\beta}\Big[\ln^2(\gamma)+4Li_2(-\gamma)+2\zeta(2)\Big] \,, \\
G_6 &= \ln\left(-\frac{t}{m^2}\right)\ln\left(\frac{(t-m^2)^2}{m^2s}\right)+2Li_2\left(\frac{t}{m^2}\right) \,, \\
G_7 &= \ln\left(\frac{(t-m^2)^2}{m^2s}\right) \,, \qquad G_8=\ln^2\left(\frac{-t}{m^2}\right) \,, \\
\gamma &= \frac{1-\beta}{1+\beta} \,, \quad \beta=\sqrt{1-4m^2/s} \,.
\end{aligned}
\qquad (45)
$$

$$
\begin{aligned}
\overline{|M^V|^2}^{fin}_{gg,int} &= \mathcal{T}_W^2 \frac{2}{C_A} \frac{e^2\kappa^2}{N^2-1} \times \Bigg[\Big\{ H_1(t) \Big(9m^4 + 2t^2 + 2tu + u^2 - 6m^2(t+u) \Big) \\
&+ \frac{H_2(t)}{4(t-m^2)^2} \Big(-9m^8 + t^2u(2t+u) - 2m^2tu(3t+u) + 2m^6(5t+3u) \\
&- m^4(3t^2 - 2tu + u^2) \Big) + u \leftrightarrow t \Big\} + \frac{H_3}{4} \Big(18m^4 + 3t^2 + 4tu + 3u^2 - 12m^2(t+u) \Big) \\
&+ \frac{H_4}{4(4m^2-s)^2} \Big(-32m^8 + 4m^6(t+u) - (t+u)^2(t^2 + 4tu + u^2) \\
&+ m^4(6t^2 + 44tu + 6u^2) + 2m^2(t^3 - 3t^2u - 3tu^2 + u^3) \Big) + \frac{H_5}{s(4m^2-s)^2} \\
&\Big(80m^{10} - 32m^8(t+u) + 8m^2tu(t+u)^2 - 16m^6(t^2 + 5tu + u^2) \\
&- (t+u)^3(3t^2 + 4tu + 3u^2) + 2m^4(5t^3 + 31t^2u + 31tu^2 + 5u^3) \Big) \\
&- \frac{H_6}{4(t-m^2)^2(u-m^2)^2} \Big(18m^{12} - 34m^{10}(t+u) - t^2u^2(t^2 + 4tu + u^2) \\
&+ m^8(25t^2 + 36tu + 25u^2) + 2m^2tu(t^3 + 6t^2u + 6tu^2 + u^3) \\
&- 4m^6(2t^3 + t^2u + tu^2 + 2u^3) + m^4(t^4 - 8t^3u - 20t^2u^2 - 8tu^3 + u^4) \Big) \\
&+ \frac{H_7}{4(t-m^2)(u-m^2)(4m^2-s)} \Big(-28m^{10} + 8m^6tu + 26m^8(t+u) \\
&+ tu(t^3 + t^2u + tu^2 + u^3) - m^4(5t^3 + 23t^2u + 23tu^2 + 5u^3) \\
&+ m^2(t^4 + 4t^3u + 10t^2u^2 + 4tu^3 + u^4) \Big) \Bigg] \qquad (46)
\end{aligned}
$$

where

$$
\begin{aligned}
H_1(t) &= \frac{1}{8}\Bigg(2\mathcal{R}e\mathcal{D}_s \ln\left(\frac{-t}{m^2}\right)\ln\left(\frac{(m^2-t)^2}{m^2 s}\right) \\
&\quad +2\mathcal{I}m\mathcal{D}_s\pi \ln\left(\frac{(m^2-t)^2}{m^2 s}\right) + 4\mathcal{R}e\mathcal{D}_s Li_2\Big(\frac{t}{m^2}\Big) \\
&\quad -\mathcal{R}e\mathcal{D}_s \ln\left(\frac{-t}{m^2}\right)^2 - 2\mathcal{I}m\mathcal{D}_s\pi \ln\left(\frac{-t}{m^2}\right)\Bigg), \\
H_1(u) &= \frac{1}{8}\Bigg(2\mathcal{R}e\mathcal{D}_s \ln\left(\frac{-u}{m^2}\right)\ln\left(\frac{(m^2-u)^2}{m^2 s}\right) \\
&\quad +2\mathcal{I}m\mathcal{D}_s\pi \ln\left(\frac{(m^2-u)^2}{m^2 s}\right) + 4\mathcal{R}e\mathcal{D}_s Li_2\Big(\frac{u}{m^2}\Big) \\
&\quad -\mathcal{R}e\mathcal{D}_s \ln\left(\frac{-u}{m^2}\right)^2 - 2\mathcal{I}m\mathcal{D}_s\pi \ln\left(\frac{-u}{m^2}\right)\Bigg), \\
H_2(t) &= \mathcal{R}e\mathcal{D}_s \ln\left(\frac{-t}{m^2}\right), \qquad H_2(u) = \mathcal{R}e\mathcal{D}_s \ln\left(\frac{-u}{m^2}\right), \\
H_3 &= \zeta(2)\mathcal{R}e\mathcal{D}_s, \qquad H_4 = \mathcal{R}e\mathcal{D}_s ln\left(\frac{s}{m^2}\right), \\
H_5 &= \frac{1}{8}\Big(\frac{\mathcal{R}e\mathcal{D}_s}{\beta}\ln^2(\gamma) + \frac{4}{\beta}\mathcal{R}e\mathcal{D}_s Li_2(-\gamma) + \frac{2\mathcal{R}e\mathcal{D}_s}{\beta}\zeta(2)\Big), \\
H_6 &= \mathcal{I}m\mathcal{D}_s\pi, \qquad H_7 = \mathcal{R}e\mathcal{D}_s.
\end{aligned}
\tag{47}
$$

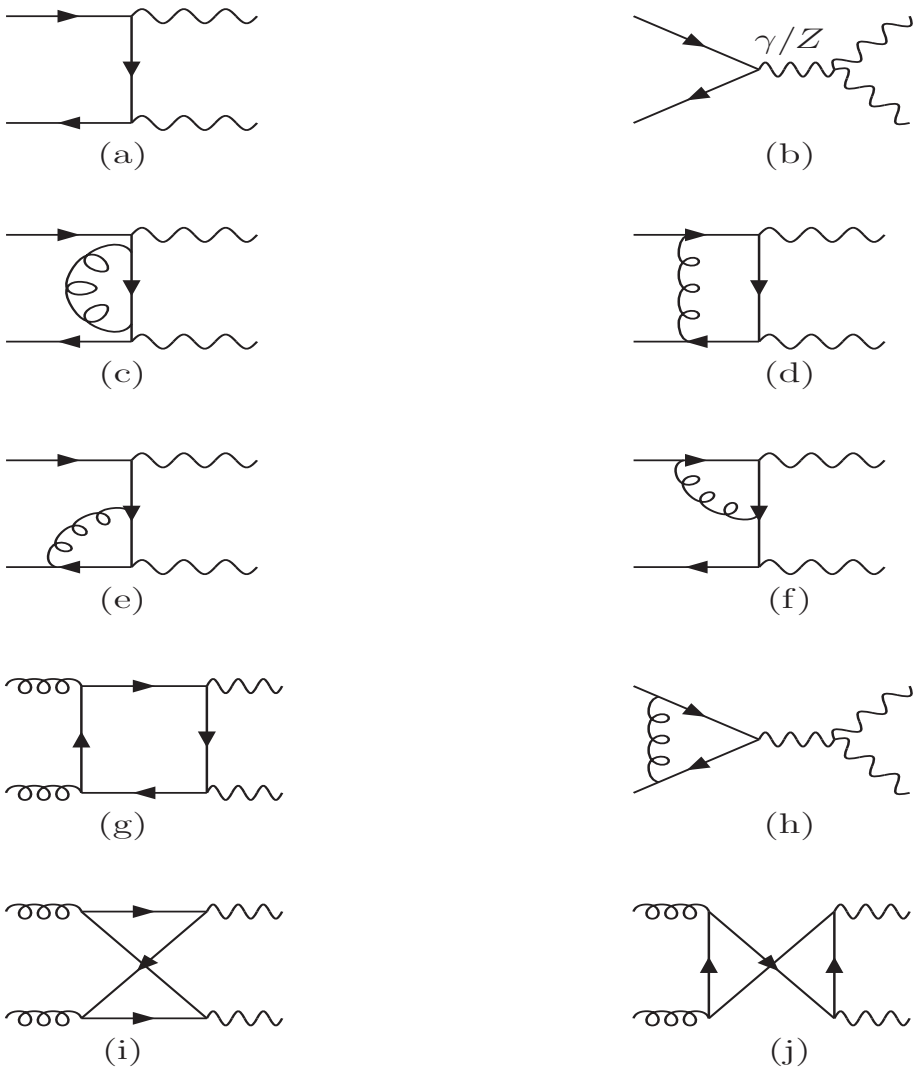

Figure 10: Leading order and order a_s virtual diagrams in SM for the subprocess $u\bar{u} \to W^+W^-$ and $gg \to W^+W^-$. The diagrams for the subprocess $d\bar{d} \to W^+W^-$ are obtained by replacing $u \to d$ and $W^+ \leftrightarrow W^-$ in the diagrams shown here.

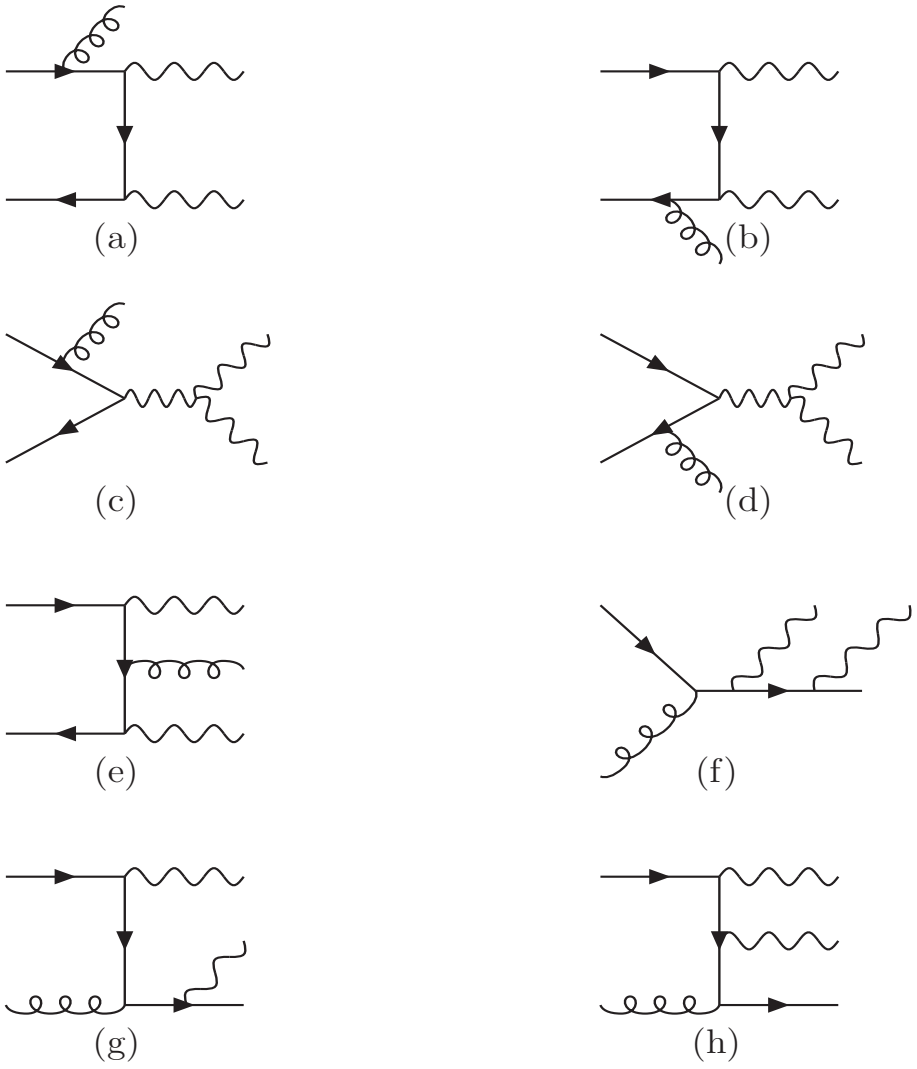

Figure 11: Order a_s real emission Feynman diagrams in SM for the subprocess $u\bar{u} \to W^+W^-g$ and $ug \to W^+W^-u$. The diagrams for the subprocess $d\bar{d} \to W^+W^-g$ and $dg \to W^+W^-d$ are obtained by replacing $u \to d$ and $W^+ \leftrightarrow W^-$ in the diagrams shown here.

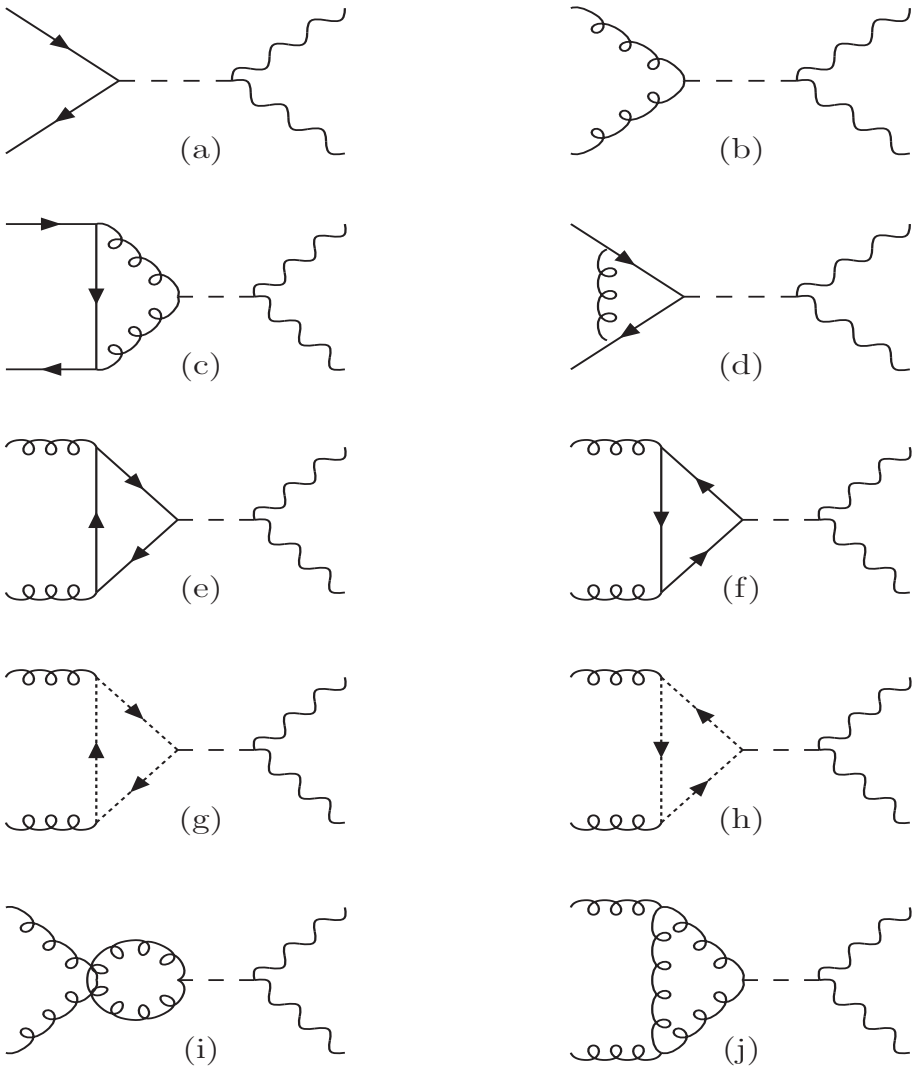

Figure 12: Leading order and order a_s gravity mediated virtual correctionss for the subprocess $q\bar{q} \to W^+W^-$ and $gg \to W^+W^-$. The big dashed lines represent gravitons and the small dashed lines represent QCD ghosts.

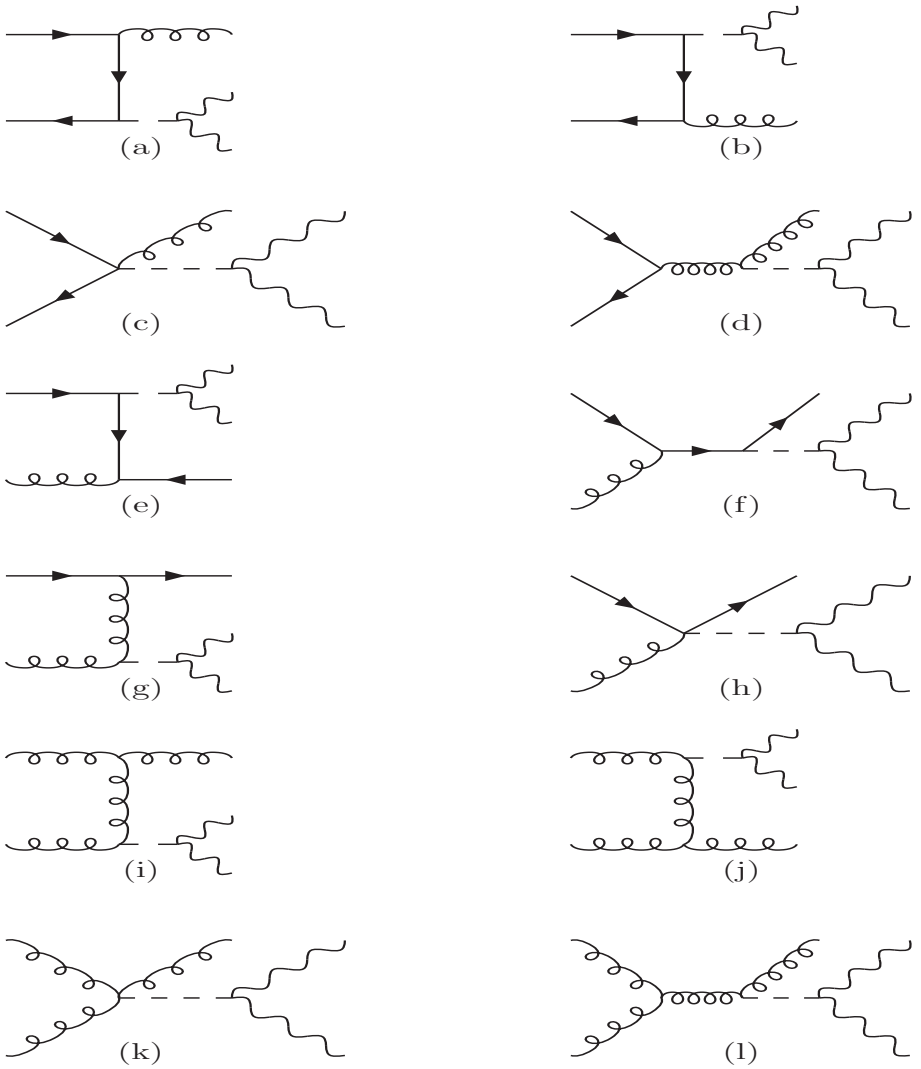

Figure 13: Gravity mediated real emission diagrams for the subprocess $q\bar{q} \to W^+W^-g$, $qg \to W^+W^-u$ and $gg \to W^+W^-g$. The big dashed lines represent gravitons.